Size-Selective Surface Organometallic Chemistry on Cagelike Mesoporous Silica

Clemens Zapilko, Yucang Liang, and Reiner Anwander*

Kjemisk Institutt, Universitetet i Bergen, Allegaten 41, 5007 Bergen, Norway

Received December 19, 2006. Revised Manuscript Received April 3, 2007

Periodic mesoporous silicas SBA-1, SBA-2, and SBA-16 feature a unique cagelike pore topology consisting of large supercages interconnected by smaller windows. Compared to channel-like mesoporous silica MCM-48, these cagelike silicas display a distinct reactivity toward magnesium silylamides $\{Mg[N(SiHMe_2)_2]_2\}_2$ and $\{Mg[N(SiMe_3)_2]_2\}_2$. All surface silanol groups ≡Si−OH of MCM-48 can be derivatized with the magnesium grafting precursors, forming stable silicon−oxygen−magnesium linkages. The completeness of the reaction is evidenced by a dramatic loss of specific pore volume (0.92 → 0.27 and 0.30 $cm^3\ g^{-1}$), disappearance of the OH stretching vibration in the IR spectrum and the magnesium content (3.5 and 4.0 wt %) of the hybrid materials $Mg[N(SiHMe_2)_2]_x$@MCM-48 and $Mg[N(SiMe_3)_2]_x$@MCM-48. In contrast, the amount of magnesium that can be grafted onto the surface of cagelike silica SBA-1 does not exceed 0.3 wt %. The specific pore volume of SBA-1 hybrid materials is only slightly decreased compared to the MCM-48 materials and the majority of the SiOH groups is still visible in the IR spectrum. We assume that the surface reaction is limited to the external surface of the SBA-1 silica particles. The remaining silanol functional groups located at the internal surface of SBA-1 are prone to further derivatization with small silylating reagents or small metalorganic compounds such as $HN(SiHMe_2)_2$ or $Ti(NMe_2)_4$ yielding organic/metalorganic or heterobimetallic hybrid materials, respectively.

Introduction

Like microporous zeolitic materials periodic mesoporous silicas (PMS)[1] can be classified according to their pore configuration. PMSs such as MCM-41,[1] SBA-15,[2] SBA-3,[3] or MCM-48[4] feature a porous structure consisting of linear, unbranched (e.g., SBA-15), or 3D-interconnected channels (MCM-48) of uniform diameter (Figure 1). In contrast, the porous network of cagelike PMSs accommodates mesosized, spherical or ellipsoidal supercages (3−9 nm) that are three-dimensionally linked by smaller channels or windows (Figure 1), as evidenced for SBA-1,[3] SBA-6,[5] SBA-12,[2] SBA-2,[3] SBA-16,[2] KIT-5,[6] FDU-12,[7] or AMS-8.[8] The diameter of the channels can vary in a wide range from molecular size (e.g., as small as 4 Å in SBA-16[9]) up to 9 nm in FDU-12.[7]

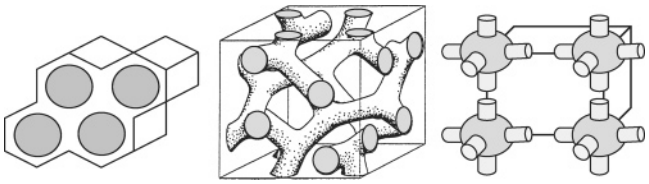

Figure 1. Schematic representation of the porous structure of MCM-41, MCM-48, and the 3D interconnected super cages in cagelike mesoporous silicas (from left to right).

Cagelike PMSs with small channels are supposed to narrow the gap between microporous zeolites and truly mesoporous structures. As a consequence, shape selectivity, which is a well-established phenomenon of zeolitic structures, could be a viable approach for medium-sized molecules and simultaneously be combined with a prolific PMS intrapore chemistry.[10] SBA-1, SBA-2, and SBA-16 are such PMS materials closely related to cagelike zeolites, albeit the pore walls are amorphous. The ability of SBA-2 and SBA-16 to act as size-selective molecular sieves has been demonstrated via sorption experiments with differently sized hydrocarbons[11] and via surface silylation with alkylchlorosilanes, respectively.[9]

We report here on size ("shape")-selective surface organometallic chemistry on SBA-1, SBA-2, and SBA-16. Sterically demanding metal silylamides are selectively grafted

* Corresponding author. E-mail: reiner.anwander@kj.uib.no. Fax: 47 555 89490.

(1) Kresge, C. T.; Leonowicz, M. E.; Roth, W. J.; Vartuli, J. C.; Beck, J. S. *Nature* **1992**, *359*, 710.
(2) (a) Zhao, D.; Feng, J.; Huo, Q.; Melosh, N.; Fredrickson, G. H.; Chmelka, B. F.; Stucky, G. D. *Science* **1998**, *279*, 548. (b) Zhao, D.; Huo, Q.; Feng, J.; Chmelka, B. F.; Stucky, G. D. *J. Am. Chem. Soc.* **1998**, *120*, 6024.
(3) (a) Huo, Q.; Margolese, D. I.; Leon, R.; Petroff, P. M.; Stucky, G. D. *Science* **1995**, *268*, 1334. (b) Huo, Q.; Margolese, D. I.; Stucky, G. D. *Chem. Mater.* **1996**, *8*, 1147.
(4) Morey, M. S.; Davidson, A.; Stucky, G. D. *J. Porous Mater.* **1998**, *5*, 195.
(5) Sakamoto, Y.; Kaneda, M.; Terasaki, O.; Zhao, D. Y.; Kim, J. M.; Stucky, G. D.; Shin, H. J.; Ryoo, R. *Nature* **2000**, *408*, 449.
(6) Kleitz, F.; Liu, D.; Anilkumar, G. M.; Park, I.; Solovyov, L. A.; Shmakov, A. N.; Ryoo, R. *J. Phys. Chem. B* **2003**, *107*, 14296.
(7) Fan, J.; Yu, C.; Gao, F.; Lei, J.; Tian, B.; Wang, L.; Luo, Q.; Tu, B.; Zhou, W.; Zhao, D. *Angew. Chem., Int. Ed.* **2003**, *42*, 3146.
(8) Garcia-Bennett, A. E.; Miyasaka, K.; Terasaki, O.; Che, S. *Chem. Mater.* **2004**, *16*, 3597.
(9) Kim, T.-W.; Ryoo, R.; Kruk, M.; Gierszal, K. P.; Jaroniec, M.; Kamiya, S.; Terasaki, O. *J. Phys. Chem. B* **2004**, *108*, 11480.
(10) For reviews see: (a) Thomas, J. M.; Raja, R. *J. Organomet. Chem.* **2004**, *689*, 4110. (b) Anwander, R. *Chem. Mater.* **2001**, *13*, 4419. (c) De Vos, D. E.; Dams, M.; Sels, B. F.; Jacobs, P. A. *Chem. Rev.* **2002**, *102*, 3615. (d) Thomas, J. M.; Raja, R.; Lewis, D. W. *Angew. Chem., Int. Ed.* **2005**, *44*, 6456.
(11) Garcia-Bennett, A. E.; Williamson, S.; Wright, P. A.; Shannon, I. J. *J. Mater. Chem.* **2002**, *12*, 3533.

10.1021/cm0630183 CCC: $37.00
Published on Web 05/27/2007

Table 1. Pore Characteristics and Elemental Analysis of the Parent PMS and Hybrid Materials

sample		V_p[a] ($cm^3\ g^{-1}$)	a_s(BET)[b] ($m^2\ g^{-1}$)	d_p(d_a)[c] (nm)	D_{me}[d] (nm)	C (%, w/w)	Mg/Ti (%, w/w)
Parent PMS Materials							
MCM-48 ($a = 8.95$ nm)[e]	**1**	0.92	1270	2.2(2.4)			
SBA-1 ($a = 7.81$ nm)[e]	**2**	0.77	1560	2.2(2.2)	4.2		
SBA-1 ($a = 8.51$ nm)[e]	**3**	0.84	1470	2.2(2.3)	4.6		
SBA-1 ($a = 7.95$ nm)[e]	**4**	1.14	1330	2.6(2.6)	4.4		
SBA-2 ($a = 5.0$ nm; $c = 8.06$ nm)[e]	**5**	0.69	1010	2.6(2.8)	4.7		
SBA-16 ($a = 14.23$ nm)[e]	**6**	0.40	590	3.6(4.8)[f]	10.9		
Dimethylsilylated Hybrid Materials							
$SiHMe_2$@MCM-48	**1a**	0.49	1010	1.8(1.9)		7.94	
$SiHMe_2$@SBA-1	**2a**	0.50	1240	1.6(1.7)	3.9	6.60	
$SiHMe_2$@SBA-1	**3a**	0.38	970	1.5(1.9)	4.1	7.85	
$SiHMe_2$@SBA-1	**4a**	0.65	1000	1.8(2.1)	4.1	6.43	
$SiHMe_2$@SBA-2	**5a**	0.51	780	2.2(2.6)	4.5	4.84	
$SiHMe_2$@SBA-16	**6a**	0.32	480	3.7(4.8)[f]	10.4	3.90	
Metalated Hybrid Materials							
$Mg[N(SiHMe_2)_2]_x$@MCM-48	**1b**	0.27	530	<1.5		16.06	3.5/0
$Mg[N(SiMe_3)_2]_x$@MCM-48	**1c**	0.30	620	<1.5		14.67	4.0/0
$Ti(NMe_2)_x$@MCM-48	**1d**	0.51	1190	<1.5		13.63	0/9.1
$Mg[N(SiHMe_2)_2]_x$@SBA-1	**2b**	0.61	1430	1.9(2.0)	4.0	3.07	<0.1/0
$Mg[N(SiMe_3)_2]_x$@SBA-1	**3c**	0.62	1280	2.0(2.1)	4.4	6.39	0.22/0
$Mg[N(SiHMe_2)_2]_x$@SBA-1	**4b**	0.33	610	<1.5	3.7	12.81	3.8/0
$Mg[N(SiHMe_2)_2]_x$@SBA-2	**5b**	0.60	900	2.5	4.6	4.72	0.6/0
$Mg[N(SiHMe_2)_2]_x$@SBA-16	**6b**	0.33	490	3.6(4.5)[f]	10.5	1.71	n.d.
Consecutively Grafted Materials							
$SiHMe_2$@$Mg[N(SiHMe_2)_2]_x$@SBA-1	**2d**	0.40	930	<1.5	3.8	7.33	0.2/0
$SiHMe_2$@$Mg[N(SiMe_3)_2]_x$@SBA-1	**3e**	0.41	980	1.7(1.9)	4.1	8.63	0.20/0
$Ti(NMe_2)_y$@$Mg[N(SiMe_3)_2]_x$@SBA-1	**3f**	0.35	810	1.6(1.7)	4.0	12.55	0.17/5.8

[a] Single-point adsorption total pore volume of pores taken at $p/p_o = 0.97$. [b] Specific BET surface area. [c] Pore diameter according to the maximum of the BJH pore size distribution calculated from the desorption (adsorption) branch of the isotherm. [d] Cage diameter according to the "model of spherical cavities" as proposed by Ravikovitch and Neimark.[22] [e] Unit-cell parameter. [f] For the SBA-16 samples, the BJH pore widths estimated from the desorption data are artifacts due to the closure of the hysteresis loop at the limiting pressure value for N_2 at 77 K.

onto the external surface of these cagelike PMSs, whereas the internal surface remains capable of further functionlization with silylating reagents or smaller-sized metal complexes. In this way, novel organic−metalorganic and heterobimetallic hybrid materials are obtained. Throughout this study, channel-like MCM-48 served as a reference system featuring a noncagelike pore topology.

Experimental Section

General. Tetraethyl orthosilicate (TEOS) from Fluka was used as a silica precursor. Mesitylene (TMB), tetramethylammonium hydroxide (25 wt % solution in water, TMAOH), octadecylbromide, hexadecylbromide, hexadecyldimethylamine, 1,12-dibromdodecane, triethylamine, (3-bromopropyl)trimethylammoniumbromide, and dibutylmagnesium (1 M in heptane) were purchased from Aldrich. 1,1,3,3-Tetramethyldisilazane and 1,1,1,3,3,3-hexamethyldisilazane were obtained from Gelest, $Ti(NMe_2)_4$ from Aldrich, and Pluronic F127 poly(ethylene oxide)−poly(propylene oxide)−poly(ethylene oxide) triblock copolymer ($EO_{106}PO_{70}EO_{106}$) from Sigma. The reagents were used as received without further purification. Octadecyltriethylammonium bromide $[CH_3(CH_2)_{17}NEt_3]^+Br^-$ (C_{18}TEABr), N-(3-trimethyl-ammoniumpropyl)hexadecylammonium dibromide $[CH_3(CH_2)_{15}NMe_2(CH_2)_3NMe_3]^{2+}2Br^-$ ($C_{16\text{-}3\text{-}1}$) and (*N*,*N*,*N*,*N*,*N*,*N*-tetramethyldihexadecyl)dodecamethylendiammonium dibromide $[CH_3(CH_2)_{15}NMe_2(CH_2)_{12}NMe_2(CH_2)_{15}CH_3]^{2+}$-$2Br^-$ ($C_{16\text{-}12\text{-}16}$) were synthesized according to the literature by reacting octadecylbromide with triethylamine, hexadecyldimethylamine with (3-bromopropyl)trimethylammonium bromide, and 1,12-dibromdodecane with hexadecyldimethylamine, respectively.[12,13] Calcined PMSs were dehydrated under a high vacuum (1×10^{-4} Torr) for 4 h at 270 °C. The syntheses of metalorganic complexes and grafting experiments were performed with rigorous exclusion of air and water, using high-vacuum and glovebox techniques (MBraun MB150B-G; <1 ppm O_2, <1 ppm H_2O). Solvents were purified by using Grubbs columns (MBraun SPS, solvent purification system). $\{Mg[N(SiMe_3)_2]_2\}_2$ **8** was synthesized according to the literature.[14]

PMS Synthesis. Periodic mesoporous silica MCM-48 **1**,[15] SBA-1 **2**−**4**,[16,17] SBA-2 **5**,[18] and SBA-16 **6**[9] were synthesized according to slightly modified literature procedures. Details of the syntheses and characterization data are given in the Supporting Information and Table 1, respectively.

Grafting Precursor $\{Mg[N(SiHMe_2)_2]_2\}_2$ 7. Dibutylmagnesium solution (3.75 mL, 3.75 mmol, 1 M in heptane) was added slowly to a solution of 1,1,3,3-tetramethyldisilazane (1.00 g, 7.50 mmol) in hexane. After being stirred for 4 h at ambient temperature, the solvent was removed in vacuo. The solid residue was crystallized from hexane at −35 °C, yielding **7** as colorless needles (1.01 g, 92%). Found: C, 33.21; H, 9.72; N, 8.75. $C_8H_{24}MgN_2Si_4$ requires: C, 33.57; H, 9.67; N, 9.68. δ_H (C_6D_6) 5.03 (sp, $^3J_{H,H} = 2.7$ Hz, 4H), 4.94 (sp, $^3J_{H,H} = 2.8$ Hz, 4H), 0.37 (d, $^3J_{H,H} = 2.7$ Hz, 24H), and 0.36 (d, $^3J_{H,H} = 2.8$ Hz, 24H) ppm; δ_C $\{^1H\}$ (C_6D_6) 6.11 and 5.14 ppm; ν_{max} (cm^{-1}) 2066s (Si−H), 1252 vs, 1052 s, 915 s, 775 m, 633 w, and 483 w.

Surface Silylation of PMS Materials. Dehydrated PMS (100 mg) was suspended in hexane and an excess of 1,1,3,3-tetramethyldisilazane (0.30 mL) was added. The mixture was stirred at

(12) Zana, R.; Benrraou, M.; Rueff, R. *Langmuir* **1991**, *7*, 1072.
(13) Widenmeyer, M. Ph. D. Thesis, Technische Universität München, Munich, Germany, 2001.
(14) Henderson, K. W.; Allan, Kennedy, A. R. *Chem. Commun.* **1997**, 1149.
(15) Widenmeyer, M.; Anwander, R. *Chem. Mater.* **2002**, *14*, 1827.
(16) Kim, M. J.; Ryoo, R. *Chem. Mater.* **1999**, *11*, 487.
(17) Vinu, A.; Murugesan, V.; Hartmann, M. *Chem. Mater.* **2003**, *15*, 1385.
(18) Hunter, H. M. A.; Wright, P. A. *Microporous Mesoporous Mater.* **2001**, *43*, 361.

ambient temperature under argon overnight and centrifuged; the separated material was washed several times with hexane and dried for 2.5 h under a vacuum. Characterization data of materials $SiHMe_2$@MCM-48 **1a**, $SiHMe_2$@SBA-1 **2a**-**4a**, $SiHMe_2$@SBA-2 **5a**, and $SiHMe_2$@SBA-16 **6a** are given in the Supporting Information and Table 1.

Grafting of Magnesium Silylamide Complexes 7 and 8. Dehydrated PMS was suspended in hexane and a solution of $\{Mg[N(SiHMe_2)_2]_2\}_2$ **7** or $\{Mg[N(SiMe_3)_2]_2\}_2$ **8** (1.5 fold excess of magnesium relative to surface silanol groups) in hexane was added. The mixture was stirred for 24 h at ambient temperature and then centrifuged; the separated white solid was washed several times with hexane and dried for 2.5 h under a vacuum. The washing fractions were combined and the solvent was removed in vacuo to isolate the unreacted metal complexes. Details of the syntheses and characterization data of materials $Mg[N(SiHMe_2)_2]_x$@MCM-48 **1b**, $Mg[N(SiMe_3)_2]_x$@MCM-48 **1c**, $Mg[N(SiHMe_2)_2]_x$@SBA-1 **2b**/**4b**, $Mg[N(SiMe_3)_2]_x$@SBA-1 **3c**, $Mg[N(SiHMe_2)_2]_x$@SBA-2 **5b**, and $Mg[N(SiHMe_2)_2]_x$@SBA-16 **6b** are given in the Supporting Information and Table 1, respectively.

$Ti(NMe_2)_x$@MCM-48 1d. MCM-48 (100 mg, 0.41 mmol SiOH groups) was suspended in hexane, and a solution of $Ti(NMe_2)_4$ (184 mg, 0.82 mmol, 2 fold excess relative to surface silanol groups) in hexane was added. The mixture was stirred for 24 h at ambient temperature and then centrifuged. The separated yellow solid was washed several times with hexane until the washing fractions were colorless and dried for 2.5 h under a vacuum to yield **1d**. FTIR: no SiOH stretching vibration. Elemental analysis found (wt %): C, 13.63, H, 3.20; N, 7.15; Ti, 9.1.

$SiHMe_2$@$Mg[N(SiHMe_2)_2]_x$@SBA-1 2d. $Mg[N(SiHMe_2)_2]_x$@SBA-1 **2b** (100 mg) was suspended in hexane, and 1,1,3,3-tetramethyldisilazane (80 mg, 0.60 mmol) was added. The mixture was then stirred at ambient temperature under argon overnight. The resulting hybrid material was centrifuged, washed several times with hexane, and dried for 2.5 h under a vacuum to yield 96 mg of **2d**. FTIR: $\nu_{SiH} = 2145\ cm^{-1}$, no SiOH stretching vibration. Elemental analysis found (wt %): C, 7.33; H, 2.18; N, 0.23; Mg, 0.2.

$SiHMe_2$@$Mg[N(SiMe_3)_2]_x$@SBA-1 3e. $Mg[N(SiMe_3)_2]_x$@SBA-1 **3c** (320 mg) was suspended in hexane and 1,1,3,3-tetramethyldisilazane (300 mg, 2.25 mmol) was added. The mixture was stirred at ambient temperature under argon overnight. The resulting hybrid material was centrifuged, washed several times with hexane, and dried for 2.5 h under a vacuum to yield 340 mg of **3e**. FTIR: $\nu_{SiH} = 2145\ cm^{-1}$, no SiOH stretching vibration. Elemental analysis found (wt %): C, 8.63; H, 2.38; N, 0.37.

$Ti(NMe_2)_y$@$Mg[N(SiMe_3)_2]_x$@SBA-1 3f. $Mg[N(SiMe_3)_2]_x$@SBA-1 **3c** (210 mg) was suspended in hexane, and a solution of $Ti(NMe_2)_4$ (250 mg, 1.2 mmol) in hexane was added. The mixture was stirred for 24 h at ambient temperature and then centrifuged. The separated yellow solid was washed several times with hexane until the washing fractions were colorless and dried for 2.5 h under a vacuum to yield **3f** (259 mg). Recovered $Ti(NMe_2)_4$: 150 mg. FTIR: no SiOH stretching vibration. Elemental analysis found (wt %): C, 12.55; H, 3.35; N, 4.67; Ti, 5.8.

Characterization. Powder X-ray diffraction (PXRD) patterns were recorded on a Philips X'pert PRO instrument in the step/scan mode (step width = 0.034; accumulation time = 30 s/step; range (2θ) = 0.31−9.96°) using monochromatic CuK_α radiation (λ = 1.5418 Å). IR spectra of the parent and silylated materials were recorded on a Perkin-Elmer FTIR spectrometer 1760X using Nujol mulls sandwiched between CsI plates. Nitrogen adsorption−desorption isotherms were measured with an ASAP 2020 volumetric adsorption apparatus (Micromeritics) at 77.4 K for relative pressures from 1×10^{-2} to 0.99 ($a_m(N_2, 77\ K) = 0.162\ nm^2$). The BET specific surface area was obtained from the nitrogen adsorption data in the relative pressure range from 0.04 to 0.2.[19] The pore size distributions were calculated using the Barrett−Joyner−Halenda (BJH) method.[20] Although the BJH method systematically underestimates the effective pore diameter of materials,[21] it gives a good measure of relative changes of the pore size. In addition, the cage diameters of the parent and hybrid materials were calculated according to the "model of spherical cavities" using equations $D_{me} = a(6\epsilon_{me}/\pi\upsilon)^{1/3}$ and $D_{me} = a(3\sqrt{3}(c/a)\epsilon_{me}/\pi\upsilon)^{1/3}$, which has been proposed by Ravikovitch and Neimark.[22] D_{me} is the diameter of the cavities of unit cells of length a (a and c), ϵ_{me} is the volume fraction of a regular cavity, $\epsilon_{me} = \rho_v V_{me}/(1 + \rho_v V_{me})$, where $\rho_v = 2.2\ g\ cm^{-3}$ is the estimated silica wall density and υ is the number of cavities per unit cell (for the *Pm3n* space group, $\upsilon = 8$, for $P6_3/mmc$ and *Im3 m* space groups, $\upsilon = 2$). Elemental analyses were performed on an Elementar VarioEL/Perkin-Elmer and a Varian SpectrAA-400. The surface silanol population was obtained from the surface coverage (SiR_3) of activated (250 °C, 3 h, 1×10^{-2} Torr) silylated samples as described previously.[23]

Results and Discussion

The pores of SBA-1 (space group *Pm3n*) consist of two different cages, forming an A_3B-type structure, with A-cages being slightly larger than B-cages. The ratio of the cage diameter is about 1.1. SBA-2 (space group $P6_3/mmc$) and SBA-16 (space group *Im3m*) exhibit a hexagonal closed arrangement of cages and a body-centered cubic structure, respectively. The number of channels connecting each cage with its nearest neighbors is lower than the theoretical maximum, and a size distribution for the channel diameter has to be taken into account.[24] The pore topology of these materials was examined in detail by electron crystallography and high-resolution transmission electron microscopy.[5,25]

The PMS materials used in this work were synthesized according to recent literature procedures.[9,15−18] For SBA-1 silicas, we employed a large headgroup surfactant, octadecyltriethylammonium bromide, affording SBA-1 **2** and SBA-1 **3**, respectively. Material SBA-1 **4** was synthesized according to a method described by Vinu et al.[17] by utilizing a prolonged hydrothermal treatment of the SBA-1 synthesis gel, 18 h instead of 1 h at 100 °C. This resulted in a considerable expansion of the pore system as derived from nitrogen physisorption data (Table 1), accompanied by a shift of the relative intensities of the (200) and (211) reflections in the powder XRD pattern (see the Supporting Information). SBA-2 **5** and SBA-16 **6** were synthesized with *N*-(3-trimethylammoniumpropyl)hexadecyldimethyl ammonium dibromide[18] and Pluronic F127 poly(ethylene oxide)−poly(propylene oxide)−poly(ethylene oxide) triblock copolymer

(19) (a) Brunauer, S.; Emmett, P. H.; Teller, E. *J. Am. Chem. Soc.* **1938**, *60*, 309. (b) Sing, K. S. W.; Everett, H.; Haul, H. R. A. W.; Moscou, L.; Pierotti, R. A.; Rouquérol, J.; Siemieniewska, T. *Pure Appl. Chem.* **1985**, *57*, 603.
(20) Barrett, E. P.; Joyner, L. G.; Halenda, P. P. *J. Am. Chem. Soc.* **1951**, *73*, 373.
(21) Zapilko, C.; Anwander, R. *Chem. Mater.* **2006**, *18*, 1479 and refs therein.
(22) Ravikovitch, P. I.; Neimark, A. V. *Langmuir* **2002**, *18*, 1550.
(23) Anwander, R.; Nagl, I.; Widenmeyer, M.; Engelhardt, G.; Groeger, O.; Palm, C.; Röser, T. *J. Phys. Chem. B* **2000**, *104*, 3532.
(24) Perez-Mendoza, M.; Gonzalez, J.; Wright, P. A.; Seaton, N. A. *Langmuir* **2004**, *20*, 7653.
(25) Zhou, W.; Hunter, H. M. A.; Wright, P. A.; Ge, Q.; Thomas, J. M. *J. Phys. Chem. B* **1998**, *102*, 6933.

Scheme 1. Proposed Surface Species Generated by Immobilization of $\{Mg[N(SiHMe_2)_2]_2\}_2$ 7 on MCM-48, Affording Hybrid Material $M[N(SiHMe_2)_2]_x$@MCM-48 1b

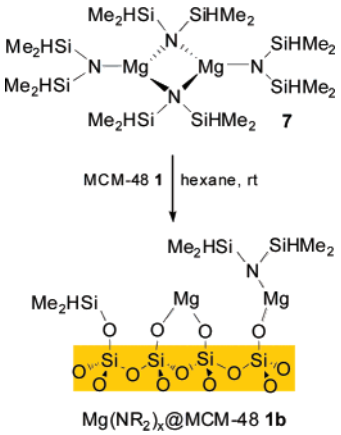

$(EO_{106}PO_{70}EO_{106})$[9] as structure-directing agents, respectively. The pore size of SBA-16 materials can be adjusted in a range of 3−9 nm.[9] The synthesis procedure employed in this study was selected to give a material with narrow pore openings. The BJH pore diameter of the SBA-1 and SBA-2 silicas are within a narrow range of 2.2−2.6 nm, and therefore we selected a MCM-48 material **1**[15] with a similar pore diameter, in order to achieve comparability for the grafting experiments.

The dehydrated materials[26] were reacted with two different magnesium silylamide complexes, new tailor-made $\{Mg[N(SiHMe_2)_2]_2\}_2$ **7** and $\{Mg[N(SiMe_3)_2]_2\}_2$ **8**[14] by exploiting the heterogeneously performed silylamide route (Scheme 1).[27] Dimeric **7** was easily synthesized from dibutylmagnesium and 1,1,3,3-tetramethyldisilazane in a way similar to the method given by Henderson et al.[14] for **8**. These hexane-soluble, molecular grafting precursors form highly dispersed, sterically unsaturated Lewis acidic surface complexes. The grafting reactions were conducted in hexane at ambient temperature under an argon atmosphere with a 1.5-fold excess of the metalorganic compound referred to by the amount of surface silanol groups[28] and followed by FTIR spectroscopy. The resulting metalorganic−inorganic hybrid materials were characterized by nitrogen physisorption and chemical analysis.

Initially, we studied the reaction of $\{Mg[N(SiHMe_2)_2]_2\}_2$ **7** with MCM-48 **1**, affording $Mg[N(SiHMe_2)_2]_x$@MCM-48 **1b**. The SiH moiety acts as an efficient IR probe to characterize and identify surface species by means of the peculiar Si−H stretching frequency. All of the FTIR-detectable SiOH groups were consumed within 18 h. The sharp band of the O−H stretch vibration at 3695 cm^{-1} vanished and a new signal at 2094 cm^{-1} with a shoulder at 2145 cm^{-1} appeared (Figure 2/B→C). These bands can be assigned to "$OSiHMe_2$" moieties (2145 cm^{-1}) and metal-bonded silylamide groups (2094 cm^{-1}, for comparison: ν_{SiH} = 2066 cm^{-1} in $\{Mg[N(SiHMe_2)_2]_2\}_2$ **7** (Figure 2/A)).

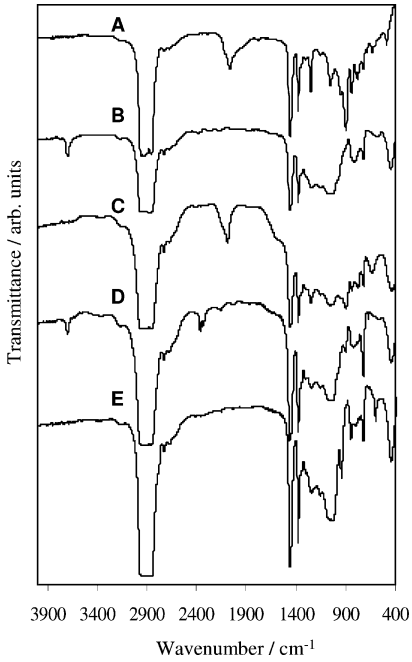

Figure 2. IR spectra (Nujol) of $\{Mg[N(SiHMe_2)_2]_2\}_2$ **7** (A), SBA-1 **2** (B), $Mg[N(SiHMe_2)_2]_x$@MCM-48 **1b** (C), $Mg[N(SiHMe_2)_2]_x$@SBA-1 **2b** (D), and $Ti(NMe_2)_y$@$Mg[N(SiMe_3)_2]_x$@SBA-1 **3f** (E).

$Mg[N(SiHMe_2)_2]_x$@MCM-48 **1b** contains 3.5 wt % magnesium, which is about half of the maximum value that should be obtained for an exclusively monopodal anchoring of magnesium to the silica surface (6.1 wt %, Scheme 1). The specific pore volume of **1b** decreased by 71% compared to the parent nonfunctionalized material and the BJH pore diameter dropped from 2.2 nm to <1.5 nm (Table 1). The shape of the adsorption−desorption isotherm changed from type IV in MCM-48 **1** to type I in **1b**, which is typical for microporous materials (Figure 3). These results indicate a uniform coverage of the pore surface with grafted magnesium complexes. $\{Mg[N(SiMe_3)_2]_2\}_2$ **8** showed a similar reaction behavior affording hybrid material **1c** (Table 1 and the Supporting Information). For comparison, dimethylsilylation of MCM-48 with 1,1,3,3-tetramethyldisilazane, yielding $SiHMe_2$@MCM-48 **1a** gave less drastic changes of pore volume (47%) and diameter (1.8 nm). Apparently, the extent of the "pore-filling" in MCM-48 is directly correlated to the size of the grafted species.

The reactions of silylamide complexes **7** and **8** with SBA-1 materials **2** and **3** proceeded in a fundamentally different way. Upon a contact time of 24 h with a hexane solution of excess $\{Mg[N(SiHMe_2)_2]_2\}_2$ **7**, the IR spectrum of $Mg[N(SiHMe_2)_2]_x$@SBA-1 **2b** still showed an intense OH stretching vibration (Figure 2/D), which is not further decreased even after 5 days of reaction. Only a very small signal at 2145 cm^{-1} assignable to $OSiHMe_2$ moieties was detected. Approximately 93% of the grafting precursor **7** could be recovered from the reaction mixture, which is reflected in the low magnesium content of **2b** (ca. 0.1%). Also, the amount of carbon is about five times lower than in $Mg[N(SiHMe_2)_2]_x$@MCM-48 **1b**. We studied the same

(26) The calcined materials were dehydrated at 270 °C for 4 h in vacuo (1×10^{-4} Torr) and stored in a glovebox.
(27) Anwander, R.; Runte, O.; Eppinger, J.; Gerstberger, G.; Herdtweck, E.; Spiegler, M. *J. Chem. Soc., Dalton Trans.* **1998**, *5*, 847.
(28) The silanol population was calculated from the carbon content of the dimethylsilylated materials (Table 1). MCM-48 **1a**, 4.09 mmol OH g^{-1}; SBA-1 **2a**, 3.27 mmol OH g^{-1}; SBA-1 **3a**, 4.04 mmol OH g^{-1}; SBA-1 **4a**, 3.17 mmol OH g^{-1}; SBA-2 **5a**, 2.28 mmol OH g^{-1}; SBA-16 **6a**, 1.79 mmol OH g^{-1}.[23]

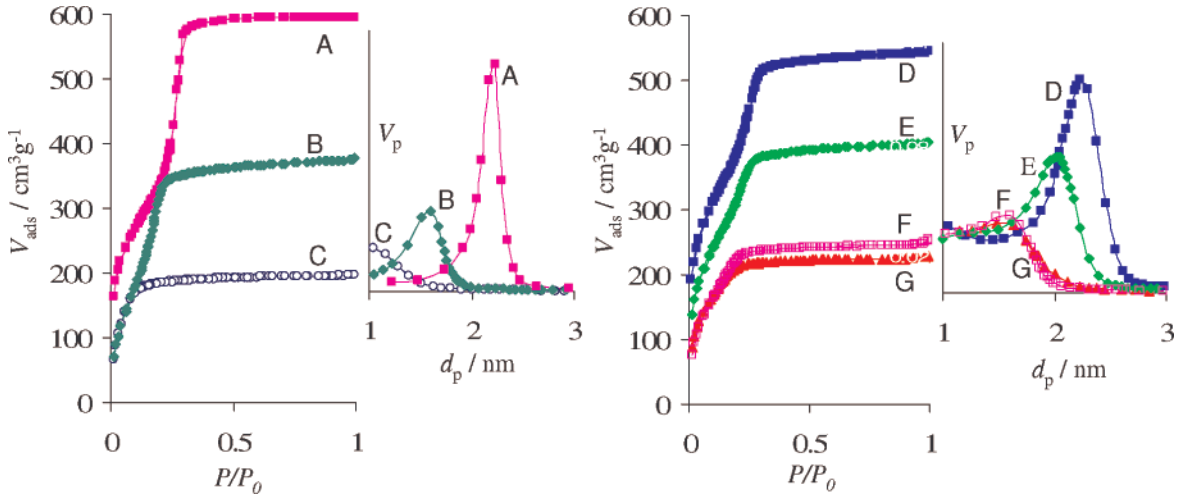

Figure 3. Nitrogen adsorption/desorption isotherms and corresponding BJH pore size distributions MCM-48 (**1**, ■ (pink), A), $SiHMe_2$@MCM-48 (**1a**, ◆ (green), B), $Mg[N(SiHMe_2)_2]_x$@MCM-48 (**1b**, □, C), left, and SBA-1 (**3**, ■ (blue), D), $Mg[N(SiHMe_2)_2]_x$@SBA-1 (**3c**, ◆ (green), E), $SiHMe_2$@SBA-1 (**3a**, □ (pink), F), $Ti(NMe_2)_y$@$Mg[N(SiHMe_3)_2]_x$@SBA-1 (**3f**, ▲ (red), G).

reaction for SBA-1 **3** with $\{Mg[N(SiMe_3)_2]_2\}_2$ **8** as a grafting reagent. Again, the vast majority of the FTIR-detectable surface OH groups is not derivatized. Correspondingly, also $Mg[N(SiMe_3)_2]_x$@SBA-1 **3c** exhibited low magnesium and carbon contents (Table 1). The nitrogen adsorption−desorption isotherms of materials $Mg[N(SiHMe_2)_2]_x$@SBA-1a **2b** and $Mg[N(SiMe_3)_2]_x$@SBA-1 **3c** are clearly of type IV with a capillary condensation step at relative pressures P/P_0 ranging from 0.1 to 0.3 (Figure 3 and the Supporting Information). Although materials **2b** and **3c** revealed a decreased specific surface area, pore volume, and BJH pore diameter, these changes are far less pronounced than in the completely dimethylsilylated SBA-1 samples $SiHMe_2$@SBA-1 **2a** and **3a**, which is opposite to the findings for MCM-48. The pore volume of the metalated SBA-1 hybrid materials **2b** and **3c** is reduced by only 21 and 26% compared with the nonfunctionalized parent silicas, respectively, whereas the corresponding MCM-48 materials show a much higher loss of pore volume (71 and 67%). We assume that the reaction of such bulky magnesium silylamido complexes with SBA-1 materials is limited to the external surface and the pore entrances of the SBA-1 particles (Scheme 2;[29] the external surface areas of parent PMS materials as derived from t-plot calculations[30] are, for SBA-1 **2**, **3**, $S_{ext} = 70$, 80 m^2g^{-1}; for MCM-48 **1**, $S_{ext} = 110$ m^2 g^{-1}). The pore openings of the SBA-1 silica framework are probably narrowed by grafted metal complexes and hence prevent nonreacted silylamide complexes from further diffusion into the porous structure. This effect is not restricted to SBA-1, but is in the same way observed for SBA-2 and SBA-16 (Table 1 and the Supporting Information) and can therefore be considered as a general phenomenon of cagelike PMSs with narrow pore openings.[31] These results closely resemble the reaction behavior of zeolite mordenite ($d_p \leq 0.7$ nm) toward magnesium alkyls as reported by the Basset group.[32] They achieved an efficient pore size engineering by grafting of dineopentylmagnesium onto the pore openings and the external surface of the zeolite crystallites.

To further corroborate our findings, we reacted the pore-enlarged material SBA-1 **4** with $\{Mg[N(SiHMe_2)_2]_2\}_2$ **7**, affording $Mg[N(SiHMe_2)_2]_x$@SBA-1 **4b**. A complete consumption of all IR-detectable Si−OH groups was accompanied by a strong decrease in pore volume, specific surface area, and pore diameter (Table 1 and the Supporting Information). The magnesium content (3.8%) of **4b** is almost equal to that of $Mg[N(SiHMe_2)_2]_x$@MCM-48 **1b**, indicating a similar degree of surface derivatization. This result further emphasizes the influence of the pore dimensions on the outcome of the surface reaction, for the prolonged hydrothermal treating during the synthesis of SBA-1 **4** is likely to cause an expansion of the diameter of the interconnecting channels.

Furthermore, we found that the remaining silanol groups located on the internal surface of the SBA-1 hybrid materials are still accessible to smaller grafting reagents (Scheme 2). $Mg[N(SiMe_3)_2]_x$@SBA-1 **3c** reacted smoothly at ambient temperature with 1,1,3,3-tetramethyldisilazane (approximate van der Waals size = 7.0 Å) or tetrakis(dimethylamido)-titanium(IV)[33−35] to yield the hybrid materials **3e** and **3f**.[36] The SiOH band at 3695 cm^{-1} in the IR spectra disappeared

(29) (a) Phull, H.; Alberti, D.; Korobkov, I.; Gambarotta, S.; Budzelaar, P. H. M. *Angew. Chem., Int. Ed.* ***2006***, *45*, 5331. (b) Mitzel, N. W.; Parsons, S.; Blake, A. J.; Rankin, D. W. H. *J. Chem. Soc., Dalton Trans.* **1996**, 2089.

(30) Zhu, H. Y.; Zhao, X. S.; Lu, G. Q.; Do, D. D. *Langmuir* **1996**, *12*, 6513.

(31) Size-selective surface reactions are not restricted to magnesium compounds. Grafting of yttrium silylamide $Y[N(SiHMe_2)_2]_3(thf)_2$ onto SBA-1 yields similar hybrid materials with the majority of the surface OH groups remaining underivatized.

(32) Theolier, A.; Custodero, E.; Choplin, A.; Basset, J. M.; Raatz, F. *Angew. Chem.* **1990**, *102*, 803.

(33) For a recent review on surface organometallic chemistry, see: Copéret, C.; Chabanas, M.; Saint-Arroman, R. P.; Basset, J.-M. *Angew. Chem., Int. Ed.* **2003**, *42*, 156.

(34) For grafting of titanium amide complexes on nonporous silica, see: Bough, A. O.; Rice, G. L.; Scott, S. L. *J. Am. Chem. Soc.* **1999**, *121*, 7201.

(35) Widenmeyer, M.; Grasser, S.; Köhler, K.; Anwander, R. *Microporous Mesoporous Mater.* **2001**, *44*−*45*, 327.

(36) For the generation of related bifunctionalized channellike PMS materials, see: Johnson, B. F. G.; Raynor, S. A.; Shephard, D. S.; Maschmeyer, T.; Thomas, J. M.; Sankar, G.; Bromley, S.; Oldroyd, R.; Gladden, L.; Mantle, M. D. *Chem. Commun.* **1999**, 1167.

Scheme 2. Schematic Representation of a Consecutive Grafting Experiment on SBA-1 (OH = surface silanol group, Mg (green) = grafted magnesium complex, = Si (orange) silyl group, Ti (blue) = grafted titanium complex; approximate van der Waals dimensions from crystallographic data are indicated)[29]

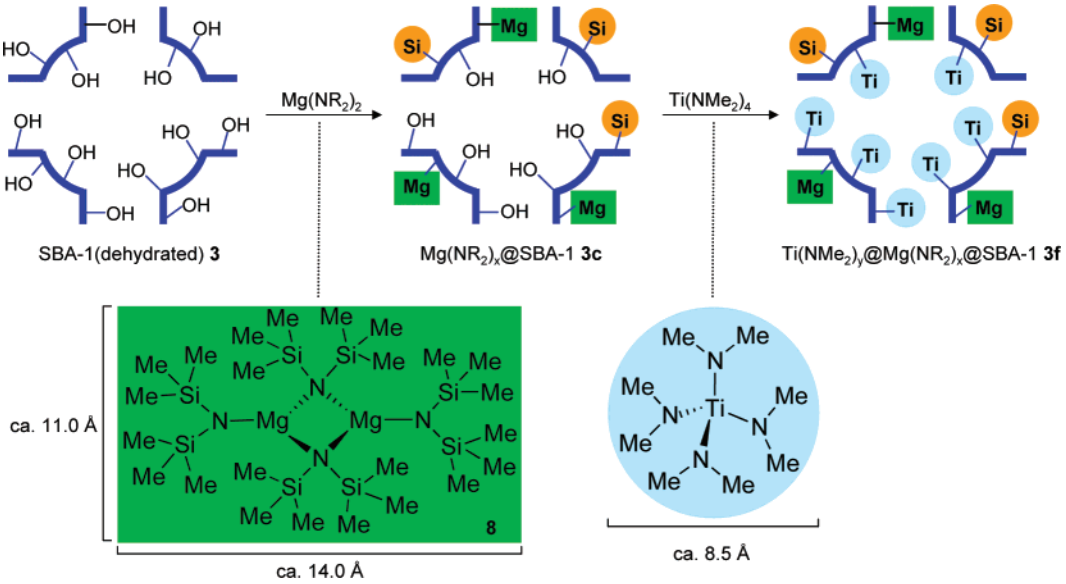

and instead bands at 2145 and 950 cm^{-1} due to $OSiHMe_2$ moieties and surface-anchored titanium complexes were observed (Figure 2/E). Nitrogen physisorption data revealed the expected drastic decrease of the specific pore parameters of materials **3e** and **3f** (Figure 2, Table 1). For example, the grafting sequence SBA-1 **3** → $Mg[N(SiMe_3)_2]_x$@SBA-1 **3c** → $Ti(NMe_2)_y$@$Mg[N(SiMe_3)_2]_x$@SBA-1 **3f** is nicely pictured by the change of the diameter of the cavities, D_{me}, which gradually decreased from 4.6 to 4.0 nm. For the bimetallic grafted material **3f**, a titanium loading of 5.8% could be achieved (cf., 9.1% for $Ti(NMe_2)_x$@MCM-48 **1d**). Comparison of the carbon content of materials $Mg[N(SiMe_3)_2]_x$@SBA-1 **3c** and $SiHMe_2$@$Mg[N(SiMe_3)_2]_x$@SBA-1 **3e** shows that ca. 25% of the surface silanol groups (0.99 mmol OH g^{-1}) is not accessible to the bulky grafting reagent $\{Mg[N(SiMe_3)_2]_2\}_2$. Accordingly, the pore entrances of SBA-1 show size (shape) selectivity in distinguishing between sterically demanding silylamide complexes and smaller silylating agents or metal compounds, resembling the shape selectivity of microporous zeolites.

Conclusions

We have shown that the grafting of pseudo-organometallic (silyl)amides $\{Mg[N(SiHMe_2)_2]_2\}_2$, $\{Mg[N(SiMe_3)_2]_2\}_2$, and $Ti(NMe_2)_4$ as well as of disilazane $HN(SiHMe_2)_2$ onto the surface of PMS materials (here, MCM-48, SBA-1, SBA-2, and SBA-16) is sensitive to pore size and pore configuration. The consecutive grafting of such differently sized (metal)-organic molecules onto "small-dimensioned" SBA-1 silica allows for a distinct functionalization of the external and intrapore surface. Accordingly, the chemical reactivity and physical properties, e.g., hydrophobicity, of the internal pore structure can be tuned without affecting the external surface of the cagelike mesoporous silica. The thereby available hybrid materials may find applications as catalysts and adsorbents featuring tailormade size (shape) selectivity.

Acknowledgment. This research is supported by the NANO-SCIENCE program of the Universitetet i Bergen. Financial support by the Deutsche Forschungsgemeinschaft and the Fonds der Chemischen Industrie is gratefully acknowledged.

Supporting Information Available: Detailed synthesis procedures, PXRD patterns, nitrogen physisorption isotherms, and IR spectra for hybrid materials **1**−**6** (PDF). This material is available free of charge via the Internet at http://pubs.acs.org.

CM0630183